Optics EXPRESS

Endcapping of high-power 3 µm fiber lasers

YIGIT OZAN AYDIN,[1,2] FRÉDÉRIC MAES,[1,2,*] VINCENT FORTIN,[1] SOULEYMANE T. BAH,[1] RÉAL VALLÉE,[1] AND MARTIN BERNIER[1]

[1] *Centre d'Optique, Photonique et Laser (COPL), Universite Laval, Québec, Québec G1V 0A6, Canada*
[2] *These authors contributed equally to this work.*
[*] *frederic.maes.1@ulaval.ca*

Abstract: Fiber tip photodegradation through OH diffusion currently limits the long term operation of high-power fiber lasers and amplifiers operating near 3 µm. To address this issue, we investigate the resistance to OH diffusion of fluoride and oxide endcaps manufactured out of ZrF_4, AlF_3, GeO_2, SiO_2 and Al_2O_3 fibers. To this extent, the endcaps are spliced at the output of a 20 W continuous-wave fiber laser operating at 2.8 µm and their degradation over a 100 h time period is monitored. While the fluoride-based endcaps underwent failure during the first 10 h, their oxide counterparts survived the experiment, although showcasing degradation which was reflected as an increase of the endface temperature over time. To overcome this issue, we propose a novel method to completely suppress OH diffusion which consists in sputtering a nanoscopic diffusion barrier film made of silicon nitride (Si_3N_4) on the output face of the endcap. The effectiveness of the approach is validated on Al_2O_3, ZrF_4 and AlF_3 endcaps which show no sign of degradation after being used for more than a 100 h at the output of a 3 µm high-power fiber laser.

1. Introduction

Fiber laser technologies are playing an instrumental role in the development of various applications [1]. However, as the output power of fiber laser systems increases, the likelihood of end-face damage increases accordingly. In the case of the well-known Yb^{3+}:silica fiber lasers operating at 1 µm, such failure is related to the fact that their output intensity exceeds the air-glass surface damage threshold, and damage occurs either due to overheating in continuous-wave (CW) regime or laser-induced breakdown due to intense pulses [2]. To mitigate this issue, fiber-based endcaps, spliced at the output of the fiber laser systems, have been developed to allow the beam to expand in a controlled manner and therefore lower its intensity below the glass' damage threshold. Such endcaps have enabled the demonstration of fiber laser systems delivering over 100 kW of output power in CW operation [3].

Fluoride-based fiber lasers provide the means to achieve powerful laser emission between 2.8 and 4 µm [4–7], although their current output power is significantly less than their silica counterparts. Yet, we recently reported an erbium-doped zirconium fluoride fiber laser delivering 42 W of CW output power at 2.83 µm which highlighted the potential of 3 µm fiber lasers for further power-scaling up to the 100 W level [4]. Such all-fiber laser sources are coveted in the development of biological tissue ablation and remote-sensing applications given their excellent overlap with the OH bond's strong vibrational absorption band, their unrivalled beam-quality as well as their compact yet rugged design [8]. Nonetheless, the widespread deployment of high-power 3 µm-class all-fiber lasers is currently hindered by the short lifetime of such laser sources due to fiber tip degradation. Contrarily to silica fiber laser systems, this issue is the direct consequence of operating within the OH absorption band at 3 µm and the hygroscopic nature of fluoride-based glasses. Through analytical modeling, it was shown that the time elapsed before catastrophic failure of the fluoride fiber tip was inversely proportional to the square of the 3 µm output power [9]. As a result, for a 20 W power level, the all-fiber cavity reported in [4] lasted

#367365 https://doi.org/10.1364/OE.27.020659
Journal © 2019 Received 13 May 2019; revised 20 Jun 2019; accepted 20 Jun 2019; published 10 Jul 2019

less than 10 h before the fiber laser's fluoride-based endcap underwent catastrophic failure due to OH diffusion.

To address this issue, this work investigates the efficiency of different endcap materials to mitigate fiber tip degradation of 3 µm-class high-power fluoride fiber lasers. To this extent, we monitored over a 100 h time period the degradation of endcaps made out of fluoride-based glass fibers (zirconium and aluminum fluoride), oxide-based glass fibers (fluorogermanate and silica) as well as single crystal sapphire fibers when spliced at the output of a high-power fiber laser operating near 3 µm. Upon experimentation, fluoride-based endcaps underwent catastrophic failure after less than 10 h during the test, suggesting they should only be used in low-power (Watt - level) 3 µm fiber laser systems. Although the oxide and crystal-based endcaps survived the 100 h long experiment, they showcased a significant rise of their temperature over time, hence indicating they should only be used in medium-power (20 W - level) fiber laser systems to ensure long term operation. Finally, this work proposes a definitive method to suppress OH diffusion within any type of endcap material by using an efficient OH diffusion barrier. This method, which consists in sputtering a thin-film of silicon nitride (Si_3N_4) on the output face of the endcap, was validated on ZrF_4, AlF_3 and Al_2O_3 endcaps which have shown no sign of degradation under high-power 3 µm radiation over more than 100 h of experimentation.

2. Experimental setup

The home-made high-power 3 µm-class fiber laser used to investigate the degradation of the different endcap materials is depicted in Fig. 1 and is similar to the system reported in [4]. Briefly, it is made out of a 6.5 m double-clad 7 mol % erbium-doped fluorozirconate (Er^{3+}:ZrF_4) fiber manufactured by *Le Verre Fluoré*. The 15 µm diameter core of the fiber has a numerical aperture of 0.12 enabling singlemode operation above 2.4 µm. The fiber laser cavity is bounded by two intracore fiber Bragg gratings (FBGs) written through the polymer of the fiber using femtosecond pulses with the scanning phase-mask technique [10,11]. The entrance high-refectivity (HR) FBG has a reflectivity > 99 % at 2.825 µm while the output low-reflectivity (LR) FBG has a reflectivity of 8 %. The active fiber and the HR and LR-FBGs were spooled on a 32 cm diameter grooved and fan cooled aluminum spool, and secured with UV-cured polymer.

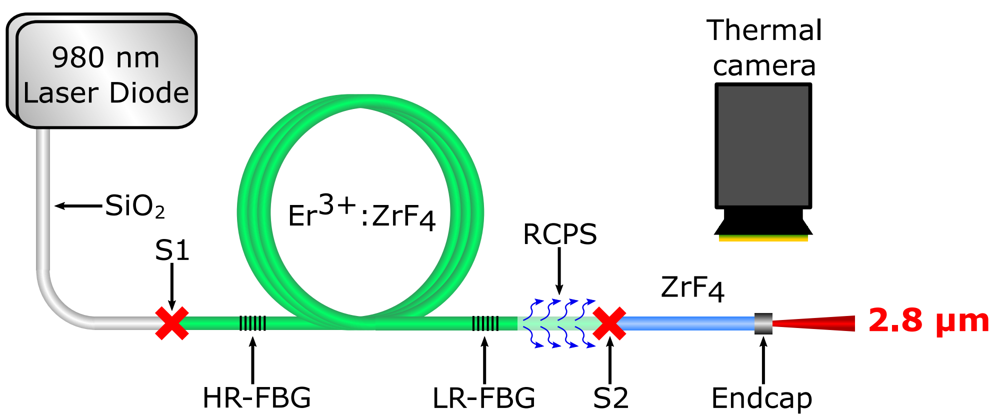

Fig. 1. Experimental setup used to monitor the degradation over time of the different endcaps when subjected to 20 W of output power at 3 µm.

In contrast to the system reported in [4], the system was solely pumped from the forward end by a 135 W commercial InGaAs 980 nm multimode laser diode whose silica delivery fiber was fusion-spliced (S1) to the Er^{3+}:ZrF_4 fiber. At the output of the fiber laser cavity, a residual cladding pump stripper (RCPS) was fabricated by applying high-index UV-cured polymer on

Optics EXPRESS

the bare Er^{3+}:ZrF_4 fiber. This pumping scheme enabled an efficiency of 23 % with respect to the launched pump and a pump power limited maximum output power of around 29 W at 2.825 µm. A singlemode fusion-splice (S2) was made between the output Er^{3+}:ZrF_4 fiber and a mode-matched passive ZrF_4 relay fiber to carry out multiple endcap degradation experiments. The relay fiber has a 15 µm core diameter, a numerical aperture of 0.12 and a 250 µm cladding diameter. The high-power all-fiber laser cavity was operated at an output power of around 20 W for all degradation experiments.

The degradation over time of the various endcaps was monitored by measuring the temperature of the endcaps' output face with a thermal camera (Jenoptik, Variocam) equipped with a close-up lens. Simultaneously, the output power of the laser system was recorded with a thermopile detector (Gentec E-O, UP25N-250F-H12-D0) to ensure it operated at a 20 W output power level throughout the experiment. It should be noted that the laser cavity was operated at this power level with the same nominal performances for over 800 h during these experiments with a stability similar to the one showcased in [4], i.e. RMS fluctuations less than 0.1%.

3. Endcap splicing and manufacturing

In this investigation, we studied the degradation of 6 different endcap fiber materials: fluorozirconate (ZrF_4 - BaF_2 - LaF_2 - AlF_3 - NaF - SrF_2 - HfF_4), fluoroaluminate (AlF_3 - $AlCl_3$ - NaF - ZrF_4 - YF_3 - SrF_2 - BaF_2 - LaF_2), fluorogermanate (GeO_2 - ZnO - PbO - K_2O - PbF_2), silica (SiO_2) and sapphire single crystal (Al_2O_3). All endcap materials were provided in fiber (or single crystal fiber) form and their specifications are presented in Table 1. The silica fiber was home-drawn using a *Heraus* preform composed of a F-300 pure silica core and a F-320 fluorine-doped silica cladding [15]. Manufacturing an endcap out of a 50 %-doped Er^{3+}:YAG single crystal (Y_3Al5O12) fiber was also studied given the unavailability of an undoped YAG fiber. Moreover, in the remainder of this work, the endcap materials will be referred to by their main constituent, for example ZrF_4 for fluorozirconate.

Table 1. Endcap Specifications^a.

Endcap	Manufacturer	n^b	α^c [$\times 10^{-6}$K^{-1}]	T_g^d [°C]	$\emptyset_c^f$ [µm]	L^g [µm]
ZrF_4	Le Verre Fluoré	1.49	17.2	265	200	480
AlF_3	Fiberlabs	1.46	18.6	390	200	450
GeO_2	Infrared Fiber Systems	1.83	10.9	420	230	380
GeO_2	Le Verre Fluoré	1.83	10.9	420	230	410
SiO_2	Heraeus F-300	1.42	0.55	1175	242	190
Er^{3+}:YAG	Shasta Crystals	1.79	6.14	T_f = 1940 ^{e}	220	320
Al_2O_3	Shasta Crystals	1.72	5 - 5.6	T_f = 2030 ^{e}	240	N.A.

[a] Optomechanical properties taken from [12–15].
[b] Refractive index around 3 µm.
[c] Thermal expansion coefficient.
[d] Transition temperature.
[e] Melting temperature.
[f] Core diameter.
[g] Length.

The endcaps were fusion-spliced to the passive ZrF_4 relay fiber using a Vytran GPX system equipped with an iridium filament (Vytran, FRAV4). For the ZrF_4 endcap, the filament was positioned at the splice point between the relay fiber and the endcap fiber. All other fibers were spliced to the ZrF_4 relay fiber by offsetting the longitudinal position of the filament in direction of the endcap fiber material as detailed in [16]. Once the fusion splice was achieved, the endcap fiber material was cleaved at a given length with a Vytran LDC cleaver. Images of the final

Optics EXPRESS

endcaps resulting from this manufacturing process are presented in Figs. 2(a)–2(c). Typical output power losses at 2.83 µm after splicing the fluoride and GeO_2 endcaps were around 4% and 8%, respectively, including fiber transmission losses and Fresnel reflections at the output endcap face and splice interface. Prior to the degradation tests, the assembly was secured using a low-index UV-cured polymer in a copper V-groove to ensure good heat conduction from the endface to the heat sink. Special care was taken to limit the length of the endcap protruding out of the copper V-groove. In contrast to natural convection, which was used in the past to study the degradation of ZrF_4 fiber tips [9], thermal conduction was chosen in the current experiment given this cooling method is more efficient, thus limiting at maximum the endface temperature.

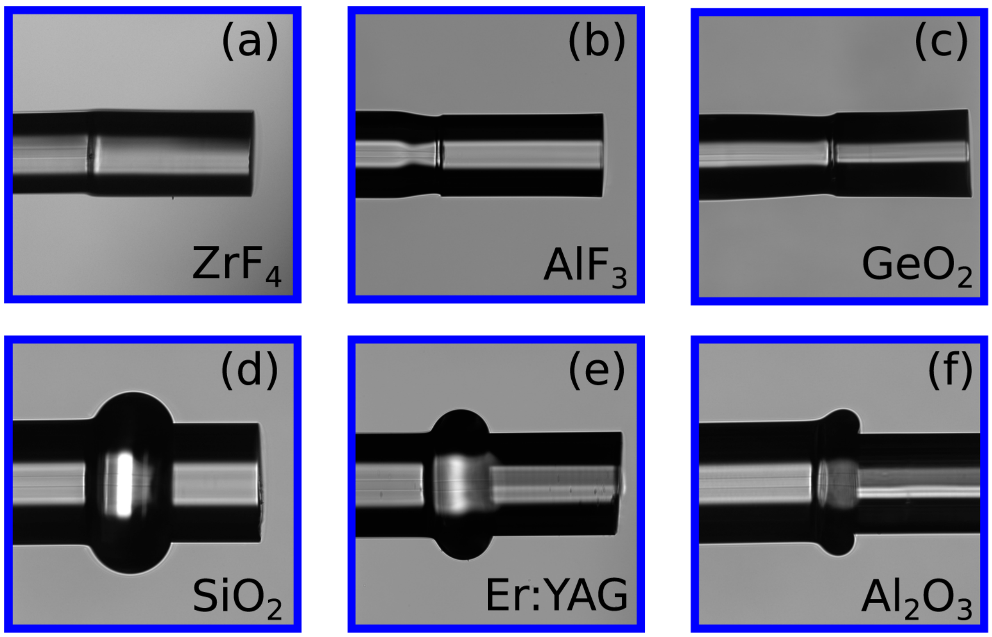

Fig. 2. Photographs of the different endcaps taken with the imaging system of the Vytran GPX.

In contrast to fluoride and GeO_2 fibers, the SiO_2, Er^{3+}:YAG and Al_2O_3 fibers form no thermal bonds when spliced to the ZrF_4 glass fiber. To overcome this limitation, we relied on the fact that the thermal expansion of ZrF_4 glass is significantly larger than that of all the oxide-based fiber materials tested, as seen in Table 1. Hence, by pushing in a controlled manner the oxide-based fiber material into the ZrF_4 fiber, after the former has been heated sufficiently, a permanent and robust joint is created as seen in Figs. 2(d)–2(f). The joint's strength is provided by the ZrF_4 glass which tightly wraps around the oxide-based fiber material once the splice point cools down. In fact, all fusion-splices resulting from this splice procedure were proof-tested at a tension of 200 g (roughly 4.4 MPa) prior to being used in the tests. It should be noted that this splicing method was also used to achieve the splice (S1) between the silica delivery fiber of the InGaAs multimode laser pump diode and the active Er^{3+}:ZrF_4 fiber shown in Fig. 1. A similar splicing method, relying on the same principle but using a CO_2 fusion-splicer, was recently shown to enable robust single-mode splices between silica and ZrF_4 fibers [17]. This principle was most-likely also employed in a number of other reports where silica and ZrF_4 fibers, or silica and chalcogenide fibers, were fusion-spliced [18–22]. The typical output power losses at 2.83 µm after splicing the SiO_2, Er^{3+}:YAG and Al_2O_3 endcaps were 8%, 10% and 16%, respectively.

In the case of the SiO_2 and Er^{3+}:YAG endcaps, it was possible to cleave the fiber material after the splice process, as seen in Figs. 2(d)–2(e), and cool the assembly in the same manner as the fluoride and GeO_2-based endcaps. It should be noted that the length of the SiO_2 endcap was shortened as much as possible due to the fiber's high absorption losses of ~ 25 dB /m near 2.825 µm. For the Er^{3+}:YAG endcap, cleaving was greatly simplified by the fact that that the crystalline planes of the Er^{3+}:YAG fiber are perpendicular to its optical axis, as shown in [23]. A photograph of the splice interface between the ZrF_4 fiber and the SiO_2 and Er^{3+}:YAG endcap is shown in Figs. 3(a)–3(b). From these images, it is clear that the interface between the SiO_2 endcap and the ZrF_4 fiber is smooth and that it does not deteriorate the quality of the laser beam. For the Er^{3+}:YAG endcap, one can see some bubbles at the interface which might degrade the beam-quality if they are located in the beam path. However, we believe optimization of the splice recipe can prevent the formation of such bubbles and enable flawless splice interfaces similar to that of the SiO_2 endcap. For the sapphire single crystal fiber, it was not possible to cleave or polish the fiber material without breaking the splice point. This stems from the fact that the crystalline planes are at 45° with respect to the optical axis of the fiber and also from it's high mechanical strength. Therefore, the whole length of the sapphire fiber (50 cm) was kept for the degradation test. Given the sapphire fiber is coreless, any attempts at cooling the fiber extremity using the copper assembly described above resulted in leakage of the 3 µm signal fom the side and the eventual failure of the assembly. Therefore, the sapphire fiber tip was tested under natural heat convection instead of heat conduction as for the other endcaps.

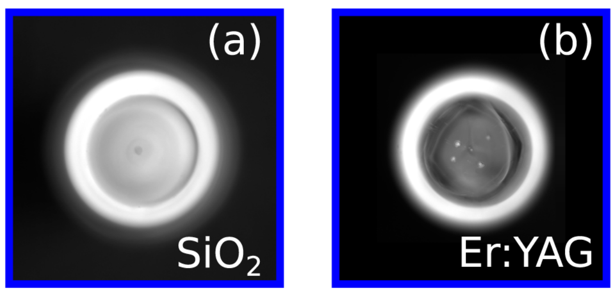

Fig. 3. Photographs of the interface between the ZrF_4 relay fiber and (a) the SiO_2 and (b) the Er^{3+}:YAG endcaps.

4. Results and discussion

4.1. Endcap degradation

Figure 4 showcases the degradation of the various endcaps under the action of 20 W CW output power at 2.83 µm over a 100 h time period. The initial temperature of the various endcaps varies between 40 - 75 °C, a variation accounted for by the difference of initial OH compound concentration, absorption coefficient at 2.83 µm, thermal conductivity [9] as well as their refractive index which determines the intensity of the Fresnel reflection at the endcap interface. As reported in [4], the fluoride fiber-based endcaps did not survive the experiment more than 10 h. While the initial temperature of the multimode ZrF_4 fiber endcap was the lowest of all the endcaps that were tested (40 °C), it underwent catastrophic failure after only 10 minutes. The degradation curve of the ZrF_4 endcap, as well as the time elapsed before failure, are in agreement with the results found in [9]. It should be noted that in the latter, the fiber tip experienced natural heat convection which increased the thermal resistance between the fiber and its surroundings, and resulted in an accelerated degradation rate. As for the AlF_3 endcap, it survived for about 10 h under similar conditions given its glass matrix is more than ten times more stable in water than that of ZrF_4 [24].

It is therefore clear that AlF_3, and even more so ZrF_4,-based endcaps are not suitable long term solutions when dealing with output powers above a few watts around 3 µm. Based on the different reports having used AlF_3 endcaps to protect fiber laser systems from photo-degradation [25,26], it can be stated that AlF_3 endcaps should be restricted to 3 µm fiber laser systems delivering output powers of a few watts in order to guarantee their long term operation. On the other hand, multimode ZrF_4 fiber endcaps should only be used in low-power systems where the output power is kept below the watt-level range. However, due to their perfectly matched refractive index, ZrF_4 endcaps produce the lowest splice interface reflection among all the tested endcaps; a significant advantage for mode-locked and in-amplifier supercontinuum Er^{3+}:ZrF_4 fiber laser systems. In both cases, the performance of these systems is greatly limited by parasitic lasing at 2.8 µm and it is therefore paramount to use an endcap producing the lowest possible feedback [27,28].

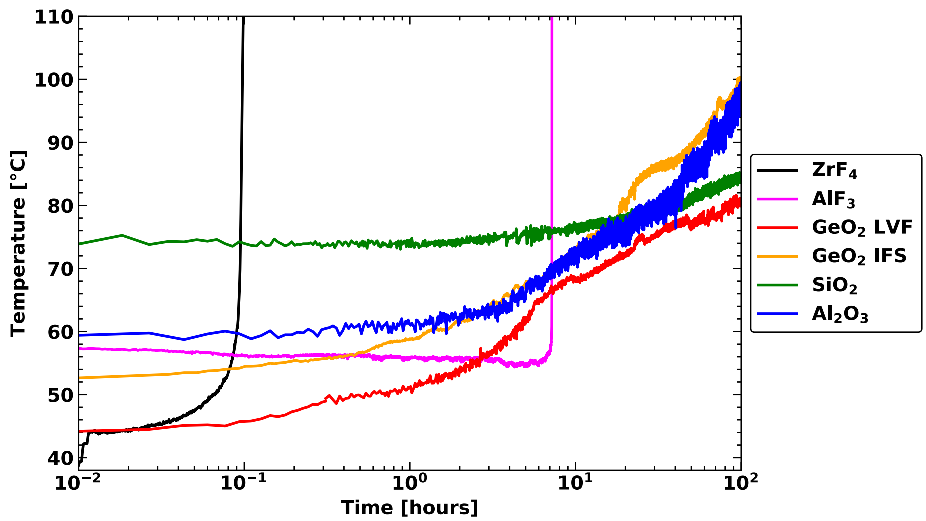

Fig. 4. Measured temperature of the endcaps' output face as a function time for a constant 3 µm output power of 20 W.

From Fig. 4 it can be seen that all the oxide-based and crystalline endcaps that were tested survived the 100 h long degradation experiment. However, the experiment also revealed that their temperature increased over time, hence indicating the existence of some degradation phenomenon. Table 2 summarizes the degradation performance of the SiO_2 and GeO_2-based endcaps. The initial temperature of the SiO_2 endcap (74 °C) is significantly higher than that of the GeO_2 endcaps (≈ 50 °C), a direct result of the strong absorption of SiO_2 around 3 µm. Given the constant ambient temperature during the experiment of 20 °C, the initial temperature rise of the SiO_2 endcap per watt of output power at 3 µm is found to be 2.7 °C/W while that of GeO_2 endcaps is roughly twice less, i.e. 1.4 °C/W. Hence, in the perspective of power-scaling the output power of 3 µm-class all-fiber lasers to 100 W, we can expect a SiO_2 endcap to reach an initial temperature of 290 °C while the temperature of a GeO_2 endcap would be between 140 - 218 °C. This allows us to conclude that GeO_2 endcaps are better candidates for high-power 3 µm systems since the splice between the SiO_2 endcaps and the ZrF_4 fiber cannot sustain temperatures in excess of the transition temperature of ZrF_4 (i.e. 270 °C [12]). Nonetheless, for medium-power systems (≈20 W), SiO_2 fibers could be considered a better alternative than GeO_2 fibers, given their degradation rate is more than three times slower than that of GeO_2. This fact has enabled the SiO_2 endcap to reach after 100 h a similar final temperature as the GeO_2 (*LVF*) endcap although their initial temperature difference was 33 °C. Moreover, SiO_2 fibers, comparatively to GeO_2 fibers, are less expensive and significantly easier to handle and process. Additionally, the refractive index of SiO_2 around 3 µm (1.42) is closer to the refractive index of ZrF_4 glass (1.49) than that of GeO_2 (1.83). This characteristic also favors SiO_2 endcaps in the design of powerful MIR mode-lock or in-amplifier fiber lasers [27,28], as discussed earlier. It should be noted that both GeO_2 endcaps that were tested behaved similarly during the experimentation, although the endcap manufactured out of the fiber provided by *Le Verre Fluoré* had a lower initial temperature. However, it is difficult to assess if this is the result of a less OH diffusion prone glass composition or a more efficient cooling.

Table 2. SiO_2 and GeO_2 Endcap Performances.

Endcap	T_i [a] °C	$\Delta T_i / \Delta P$ [b] ° C / W	$T_{i,100W}$ [c] ° C	$\Delta T / \Delta t$ [d] ° C
GeO_2 LVF	44	1.20	140	0.37
GeO_2 IFS	53	1.65	218	0.47
SiO_2	74	2.70	290	0.10

[a] Initial temperature.
[b] T_i variation with 3 µm output power.
[c] Extrapolated T_i at 100 W of output power.
[d] Temperature variation over time.

As stated earlier, the Al_2O_3 fiber tip surprisingly showed signs of degradation over time under the influence of high power 3 µm laser light. The initial temperature of the Al_2O_3 fiber tip was 60 °C and its final temperature is 97 °C, which results in a 0.37 °C/h degradation rate. While the initial temperature and degradation rate of the Al_2O_3 fiber tip is comparable to those of GeO_2 endcaps, it should be noted that the former experienced natural convection instead of heat conduction, a condition which accelerates degradation by easily a tenfold [9]. Therefore, we believe Al_2O_3 endcaps are potentially an interesting solution for high-power 3 µm fiber laser systems, contingent upon the ability to manufacture endcaps out of single crystal Al_2O_3 fibers. An alternative to manufacturing such endcaps would be to inscribe depressed cladding single-mode waveguides with femtosecond pulses in the Al_2O_3 rod fiber, as shown recently in [29]. This method would preserve the beam-quality of the 3 µm fiber laser although long lengths of Al_2O_3 fiber are used for beam delivery purposes.

Similarly to fluoride-based endcaps, we believe the degradation witnessed in the SiO_2 and GeO_2 endcaps is related to ambient water vapor diffusion within the glass matrix. In both cases, the OH vapor could be incorporated into the glass matrix in the form of GeOH or SiOH groups, as discussed in [30–33]. It is unlikely that water vapor diffused within the matrix of the single-crystal Al_2O_3 fiber given the high degree of order of its crystalline matrix. Instead, we believe the temperature increase observed during the experiment is related to water vapor adsorption at the polished surface of the sapphire fiber [34]. The occurrence of water adsorption is caused by the fact that at the surface of the single-crystal sapphire fiber, the chemistry of a pure crystal does not hold given Al-O-Al compounds are deprived of neighboring compounds. This gives rise to various chemical mechanisms through which OH can bind itself to the surface and alter the latter's properties with increasing pressure, humidity, temperature and time. However, further investigations need to be conducted in order to validate how ambient OH vapor interacts with the different oxide-based and crystalline endcaps.

As for the Er^{3+}:YAG endcap, it could not be tested given its temperature at a 3 µm power level of 2.4 W was already around 120 °C. This temperature was measured at the splice point between the relay fiber and the Er^{3+}:YAG endcap. By analyzing with a near-infrared optical spectrum analyzer the output of the 2.83 µm all-fiber laser cavity, a clear, yet weak, peak at 980 nm was observed. This indicated that some residual cladding pump remained at the output of the laser cavity which was absorbed by the heavily-doped (50 %) Er^{3+}:YAG endcap and caused its excessive heating. In spite of this, we believe undoped YAG single crystal fibers are highly interesting endcap materials given they possess thermal and mechanical properties similar to Al_2O_3 fibers while simultaneously offering the possibility to be easily processed into endcaps at the tip of ZrF_4 fibers. It should also be noted that coreless calcium fluoride (CaF_2) crystals have been recently used to endcap 3 µm fiber laser systems operating at 16 W near 2.8 µm [35]. However, given the unavailability of such material to the authors, it was not possible to evaluate it's long term degradation behaviour in the current experiment.

4.2. Si_3N_4 coatings for high-power 3 µm fiber lasers

In order to inhibit in a definite manner OH diffusion within endcap materials, we propose to coat the output face of the endcap with a nanoscopic thin-film of silicon nitride (Si_3N_4). Such materials are already extensively used in electronics as a diffusion barrier for SiO_2 dielectric layers or passivation layers in flexible electroluminescent devices [36].

In this experiment, the Si_3N_4 thin-films were deposited on the facet of the endcaps using reactive ion beam-assisted double magnetron sputtering as described in [37] under a 1.46×10^{-3} Torr environment. The target material was a 6" diameter 99.99 % pure silicon disk. The temperature of the substrate was kept at 115 °C and deposition of the thin-film was done at a 0.24 nm /s. The argon gas flow was maintained at 32 sccm during the sputtering process and the reactive gas nitrogen gaz (22 sccm) was introduced into chamber by the ion source. The uniformity of the deposited thin-film was enhanced by a rotating the substrate holder at 80 rpm.

Figure 5 compares the degradation of Si_3N_4-coated and uncoated ZrF_4, AlF_3 and Al_2O_3 endcaps under the impact of 3 µm light over a 100 h long time period. For the ZrF_4 and AlF_3 endcaps, the Si_3N_4 coating had a 25 nm thickness and the output power of the 3 µm fiber laser was 7 W, while in the case of the Al_2O_3 endcaps they were 100 nm and 20 W, respectively. For both ZrF_4 and AlF_3, the coating thickness was limited to less than 1% of the wavelength to limit the Fresnel reflection given the high refractive index ($n \sim 1.95$) of Si_3N_4. Moreover, all endcaps experienced natural convection to accelerate the photodegradation process. From Fig. 5 it is clear that the Si_3N_4 coating inhibits OH diffusion for all the tested endcaps given no increase of temperature over time is recorded. It also demonstrates that Si_3N_4 coatings can be applied on a variety of fiber materials.

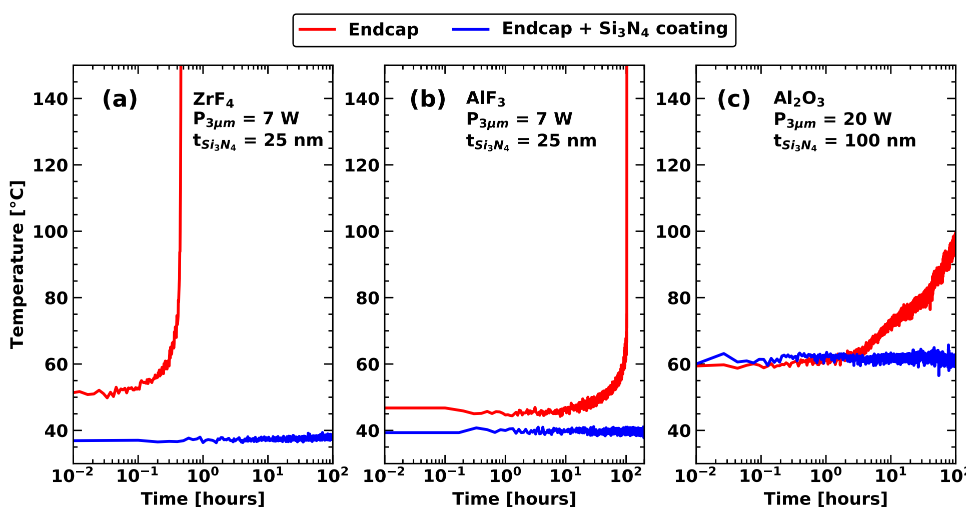

Fig. 5. Measured temperature of the (a) ZrF_4, (b) AlF_3 and (c) Al_2O_3 endcaps compared to their Si_3N_4 coated counterparts as a function of time. The 3 µm output power and Si_3N_4 coating thickness used for the ZrF_4 and AlF_3 endcaps were 7 W and 25 nm, respectively, while those for the Al_2O_3 endcap was 20 W and 100 nm, respectively.

However, some Si_3N_4 coatings showed signs of cracking a few months after their deposition upon the fibers as result of high surface stresses. Such stresses can nonetheless be relieved through the deposition of thinner Si_3N_4 thin-films. Hence, future investigation will attempt to find a thickness range where Si_3N_4 coatings do not crack over time while simultaneously preserving their OH impermeability. These investigations will also consider the introduction of oxygen within the Si_3N_4 matrix which has been show to improve its flexibility [38]. Finally, the Si_3N_4 coating optimization will also be facilitated by the number of potential endcap substrates upon which they can be deposited, i.e. ZrF_4, AlF_3, GeO_2, SiO_2, YAG and Al_2O_3. We believe that an optimized endcap properly coated with Si_3N_4 will enable the long term operation (> 10,000 h) of 100 W - level 3 µm-class fiber laser systems in the near future. It should be noted that silicon nitride or silicon oxynitride could also be used to coat the outer glass cladding of optical fibers. Such coatings could constitute a transparent alternative to thin carbon, metallic or ORMOCER coatings which have been shown to provide an excellent protection against OH diffusion within SiO_2-based fibers [39–41].

5. Conclusion

In this work, the OH degradation of various endcaps spliced at the output of a 20 W all-fiber laser at 3 µm was monitored over a 100 h time period. This investigation showed that fluoride, i.e. ZrF_4 and AlF_3,-based endcaps lasted for less than 10 h before undergoing catastrophic failure, hence indicating they should only be used for low-power applications. On the other hand, the oxide-based endcaps (GeO_2 and SiO_2) as well as the tip of a Al_2O_3 fiber survived the experiment, which makes them interesting endcap solutions for medium-power systems (~ 20 W). To the best of our knowledge, this is the first report in which oxide-based materials are spliced and processed into endcaps at the output of a fluoride fiber laser. Nonetheless, all oxide materials showcased a clear temperature increase over time, an observation which is believed to stem from OH diffusion in the GeO_2 and SiO_2 glass matrix or presumably OH adsorption in the case of Al_2O_3.

In order to inhibit OH interaction with endcap materials under the irradiation of intense 3 µm light, we also propose in this work to coat the output face of endcaps with a silicon nitride (Si_3N_4) thin-film. The effectiveness of the proposed method is demonstrated on Si_3N_4 coated ZrF_4 and AlF_3 endcaps, as well as on a Al_2O_3 fiber tip. Upon illumination with 3 µm light for a 100 h, the coated endcaps and fiber tip showed no sign of degradation, whereas their uncoated counterparts either underwent catastrophic failure (ZrF_4 and AlF_3) or showed a significant temperature rise (Al_2O_3). We believe optimized Si_3N_4-coated endcaps will allow the long-term operation of 100 W-level 3 µm class all-fiber lasers in the near future, and spark the development of cutting-edge mid-infrared applications.

Funding

Canada Foundation for Innovation (CFI) (5180); Fonds de Recherche du Québec - Nature et Technologies (FRQNT) (144616); Natural Sciences and Engineering Research Council of Canada (NSERC) (CG112389, IRCPJ469414-13).

Acknowledgements

The authors wish to thank Yannick Ledemi for insightful discussions.

References

1. W. Shi, Q. Fang, X. Zhu, R. A. Norwood, and N. Peyghambarian, “Fiber lasers and their applications,” Appl. Opt. **53**(28), 6554–6568 (2014).
2. A. Carter, B. N. Samson, K. Tankala, D. P. Machewirth, V. Khitrov, U. H. Manyam, F. Gonthier, and F. Seguin, “Damage mechanisms in components for fiber lasers and amplifiers,” Proc. SPIE **5647**, 561–571 (2004).

3. E. A. Shcherbakov, V. V. Fomin, A. A. Abramov, A. A. Ferin, D. V. Mochalov, and V. P. Gapontsev, "Industrial grade 100 kW power CW fiber laser," in *Advanced Solid-State Lasers Congress, OSA Technical Digest (online)* (Optical Society of America, 2013), paper ATh4A.2.
4. Y. O. Aydin, V. Fortin, M. Bernier, and R. Vallée, "Towards power scaling of 2.8 μm fiber lasers," Opt. Lett. **43**(18), 4542–4545 (2018).
5. V. Fortin, F. Jobin, M. Larose, M. Bernier, and R. Vallée, "10 W-level monolithic dysprosium-doped fiber laser at 3.24 μm," Opt. Lett. **44**(3), 491–494 (2019).
6. F. Maes, V. Fortin, M. Bernier, and R. Vallée, "5.6 W monolithic fiber laser at 3.55 μm," Opt. Lett. **42**(11), 2054–2057 (2017).
7. F. Maes, V. Fortin, S. Poulain, M. Poulain, J.-Y. Carrée, M. Bernier, and R. Vallée, "Room-temperature fiber laser at 3.92 μm," Optica **5**(7), 761–764 (2018).
8. S. D. Jackson, "Towards high-power mid-infrared emission from a fibre laser," Nat. Photonics **6**(7), 423–431 (2012).
9. N. Caron, M. Bernier, D. Faucher, and R. Vallée, "Understanding the fiber tip thermal runaway present in 3 μm fluoride glass fiber lasers," Opt. Express **20**(20), 22188–22194 (2012).
10. M. Bernier, D. Faucher, R. Vallée, A. Saliminia, G. Androz, Y. Sheng, and S. L. Chin, "Bragg gratings photoinduced in ZBLAN fibers by femtosecond pulses at 800 nm," Opt. Lett. **32**(5), 454–456 (2007).
11. J. Habel, T. Boilard, J.-S. Frenière, F. Trépanier, and M. Bernier, "Femtosecond FBG written through the coating for sensing applications," Sensors **17**(11), 2519 (2017).
12. X. Zhu and N. Peyghambarian, "High-power ZBLAN glass fiber lasers: Review and prospect," Adv. Optoelectron. **2010**, 1–23 (2010).
13. H. Li, J. Lousteau, W. N. Macpherson, X. Jiang, H. T. Bookey, J. S. Barton, A. Jha, and A. K. Kar, "Thermal sensitivity of tellurite and germanate optical fibers," Opt. Express **15**(14), 8857–8863 (2007).
14. Shasta Crystals, "Product catalog," (2018).
15. Heraus, "Specialty fiber preforms for the most demanding applications," https://www.heraeus.com/media/media/hqs/doc_hqs/products_and_solutions_8/optical_fiber/Specialty_Fiber_Preforms_EN.pdf.
16. S. Jiang and J. Wang, "Method of fusion splicing silica fiber with low-temperature multi-component glass fiber," U.S. patent 6,705,771 (April 16, 2004).
17. R. Carbonnier and W. Zheng, "New approach for high reliability, low loss splicing between silica and ZBLAN fibers," Proc. SPIE **10513**, 105131G (2018).
18. K. Yin, B. Zhang, J. Yao, L. Yang, S. Chen, and J. Hou, "Highly stable, monolithic, single-mode mid-infrared supercontinuum source based on low-loss fusion spliced silica and fluoride fibers," Opt. Lett. **41**(5), 946–949 (2016).
19. R. Thapa, R. R. Gattass, V. Nguyen, G. Chin, D. Gibson, W. Kim, L. B. Shaw, and J. S. Sanghera, "Low-loss, robust fusion splicing of silica to chalcogenide fiber for integrated mid-infrared laser technology development," Opt. Lett. **40**(21), 5074–5077 (2015).
20. T. Huang, Q. He, X. She, X. Shu, and C. Liu, "Study on thermal splicing of ZBLAN fiber to silica fiber," Opt. Eng. **55**(10), 106119 (2016).
21. Z. Zheng, D. Ouyang, J. Zhao, M. Liu, S. Ruan, P. Yan, and J. Wang, "Scaling all-fiber mid-infrared supercontinuum up to 10 W-level based on thermal-spliced silica fiber and ZBLAN fiber," Photonics Res. **4**(4), 135–139 (2016).
22. R. Al-Mahrous, R. Caspary, and W. Kowalsky, "A thermal splicing method to join silica and fluoride fibers," J. Lightwave Technol. **32**(2), 303–308 (2014).
23. R. Thapa, D. Gibson, R. R. Gattass, C. Askins, W. Kim, S. Bayya, L. B. Shaw, and J. S. Sanghera, "Fusion splicing of highly dissimilar YAG crystal fiber and silica fiber with reaction bonding," Opt. Mater. Express **6**(8), 2560–2566 (2016).
24. G. H. Frischat, B. Hueber, and B. Ramdohr, "Chemical stability of ZrF_4 and AlF_3-based heavy metal fluoride glasses in water," J. Non-Cryst. Solids **284**(1-3), 105–109 (2001).
25. Y. O. Aydin, V. Fortin, D. Kraemer, A. Fraser, R. Vallée, and M. Bernier, "High-energy picosecond pulses from a 2850 nm fiber amplifier," Opt. Lett. **43**(12), 2748–2751 (2018).
26. S. Duval, J.-C. Gauthier, L.-R. Robichaud, P. Paradis, M. Olivier, V. Fortin, M. Bernier, M. Piché, and R. Vallée, "Watt-level fiber-based femtosecond laser source tunable from 2.8 to 3.6 μm," Opt. Lett. **41**(22), 5294–5297 (2016).
27. J. C. Gauthier, V. Fortin, S. Duval, R. Vallée, and M. Bernier, "In-amplifier mid-infrared supercontinuum generation," Opt. Lett. **40**(22), 5247–5250 (2015).
28. S. Duval, M. Bernier, V. Fortin, J. Genest, M. Piché, and R. Vallée, "Femtosecond fiber lasers reach the mid-infrared," Optica **2**(7), 623–626 (2015).
29. J.-P. Bérubé, J. Lapointe, A. Dupont, M. Bernier, and R. Vallée, "Femtosecond laser inscription of depressed cladding single-mode mid-infrared waveguides in sapphire," Opt. Lett. **44**(1), 37–40 (2019).
30. A. J. Moulson and J. P. Roberts, "Water in silica glass," Trans. Faraday Soc. **57**, 1208–1216 (1961).
31. M. Tomozawa, H. Li, and K. Davis, "Water diffusion , oxygen vacancy annihilation and structural relaxation in silica glasses," J. Non-Cryst. Solids **179**, 162–169 (1994).
32. K. Davis, A. Agarwal, M. Tomozawa, and K. Hirao, "Quantitative infrared spectroscopic measurement of hydroxyl concentrations in silica glass," J. Non-Cryst. Solids **203**, 27–36 (1996).
33. X. Jiang, J. Lousteau, S. Shen, and A. Jha, "Fluorogermanate glass with reduced content of OH-groups for infrared fiber optics," J. Non-Cryst. Solids **355**(37-42), 2015–2019 (2009).

34. H. Knözinger and P. Ratnasamy, "Catalytic aluminas : Surface models and characterization of surface sites," Catal. Rev.: Sci. Eng. **17**(1), 31–70 (1978).
35. C. A. Schäfer, H. Uehara, D. Konishi, S. Hattori, H. Matsukuma, M. Murakami, S. Shimizu, and S. Tokita, "Fluoride-fiber-based side-pump coupler for high-power fiber lasers at 2.8 µm," Opt. Lett. **43**(10), 2340–2343 (2018).
36. A. E. Kaloyeros, F. A. Jové, J. Goff, and B. Arkles, "Review-Silicon nitride and silicon nitride-rich thin film technologies: Trends in deposition techniques and related applications," ECS J. Solid State Sci. Technol. **6**(10), P691–P714 (2017).
37. S. T. Bah, C. O. Ba, M. D'Auteuil, P. Ashrit, L. Sorelli, and R. Vallée, "Fabrication of TaO_xN_y thin films by reactive ion beam-assisted ac double magnetron sputtering for optical applications," Thin Solid Films **615**, 351–357 (2016).
38. M. Józwik, P. Delobelle, C. Gorecki, A. Sabac, L. Nieradko, C. Meunier, F. Munnik, and M. Jo, "Optomechanical characterisation of compressively prestressed silicon oxynitride films deposited by plasma-enhanced chemical vapour deposition on silicon membranes," Thin Solid Films **468**(1-2), 84–92 (2004).
39. C. A. Taylor and W. K. Chiu, "Characterization of CVD carbon films for hermetic optical fiber coatings," Surf. Coat. Technol. **168**(1), 1–11 (2003).
40. K.-H. Haas and H. Wolter, "Synthesis , properties and applications of inorganic - organic copolymers," Curr. Opin. Solid State Mater. Sci. **4**(6), 571–580 (1999).
41. D. A. Pinnow, G. D. Robertson, and J. A. Wysocki, "Reductions in static fatigue of silica fibers by hermetic jacketing," Appl. Phys. Lett. **34**(1), 17–19 (1979).